AN INTEGRATIVE APPROACH FOR MONITORING WATER MOVEMENT IN THE VADOSE ZONE

T.-C. J. Yeh
Department of Hydrology and Water Resources, The University of Arizona

S. Liu
Burgess & Niple

ABSTRACT

Electrical resistivity tomography (ERT), during the past few years, has emerged as a potentially cost-effective, non-invasive tool for imaging changes of moisture content in the vadose zone. The accuracy of ERT surveys, however, has been the subject of debate because of its non-unique inverse solution and spatial variability in the parameters of the constitutive resistivity-moisture content relation. In this paper, an integrative inverse approach for ERT, based on a stochastic information fusion concept (Yeh and ®im nek, 2002) was developed to derive the best unbiased estimate of the moisture content distribution. Unlike classical ERT inversion approaches, this new approach assimilates both prior information about the geological and moisture content structures in a given geological medium, and sparse point measurements of the moisture content, electrical resistivity, and electric potential. Using these types of data and considering the spatial variability of the parameters in the resistivity-moisture content relation, the new approach directly estimates three-dimensional moisture content distributions, instead of simply changes in moisture content in the vadose zone. Numerical results show that the integrative approach can produce accurate estimates of the moisture content distributions, and that incorporating sparse measurements of the moisture content is essential to enhance the estimate.

INTRODUCTION

Electrical resistivity surveys are increasingly used to collect extensive electric current and potential data in multi-dimensions to image the subsurface electrical resistivity distribution [1,2,3,4]. Recently, ERT surveys have found their way into subsurface hydrology applications. This is attributed to the fact that knowledge of the spatial distribution of the electrical properties of subsurface media can provide valuable information for characterizing waste sites and monitoring flow and contaminant movement in the vadose zone. For example, during an infiltration event, the moisture content of a geological medium is generally the only factor that undergoes dramatic changes and the changes in resistivity can be related to changes in moisture content. Tracking the changes in resistivity through time, therefore, has been found to be useful for detecting temporal changes in the moisture content of the vadose zone [1,5].

While ERT surveys are useful, Yeh et al. [6] showed that uncertainties in tracking moisture movement in the vadose zone, based on ERT surveys alone, can be quite significant. They suggested that both inverse modeling of the ERT surveys and the spatial variability of the parameters in the constitutive resistivity-moisture content relation contribute to the overall uncertainties. Depending upon the number of parameters to be inverted and the quantity of data available [7], the ERT survey inverse problem is often ill-posed, and may have no unique

solution. For ill-posed problems, most ERT inversion approaches employ optimization algorithms with some type of regularization (e.g., [8]). While the regularization algorithm yields smooth estimates, there is no guarantee that it will produce the best unbiased estimate of the resistivity field, which reflects of the flow process and underlying geological structures. Regularization also does not provide a meaningful way to quantify the uncertainty associated with the spatial variability. Additionally, when converting changes in resistivity to changes in moisture content, it is often assumed that the parameters in the constitutive resistivity-moisture content relation (e.g., Archie's Law) are constant over the entire domain. Recent studies by Baker [9] and Yeh, et al. [6] reported pronounced spatial variability of these parameters in the field. Neglecting this spatial variability and using a single resistivity-moisture calibration curve can add to the level of uncertainty in the final interpreted change in moisture content (in an unquantifiable way.)

Besides the uncertainties inherent in the interpretation of ERT surveys, most current three-dimensional inverse models require significant computational resources to process the large data sets typically collected during a survey. Furthermore, a change in moisture content only provides qualitative information about water movement in the vadose zone; the actual moisture content values at each point, which are vital to hydrological investigations or hydrological inverse modeling (e.g., [7]), remain unknown. For instance, since the unsaturated hydraulic conductivity is a nonlinear function of moisture content, changes in the moisture content alone do not provide enough information to uniquely characterize the unsaturated hydraulic properties of the vadose zone. As a consequence, an inverse approach is needed that can account for spatial variability in the resistivity-moisture content relation, efficiently process the large number of data sets, and produce detailed moisture content distributions with the least amount of uncertainty.

While the physical process of electric current flow is different from that of groundwater flow, the governing equation of the electric current and the potential fields created during an ERT surveys is analogous to that of steady confined groundwater flow. The mathematical treatment of the inversion of an ERT survey is therefore similar to that used in hydraulic tomography [10, 11]. Using this similarity, the sequential, successive linear estimator approach for hydraulic tomography [10], which has been validated with sandbox experiments [12], was extended recently to ERT surveys by Yeh et al. [6]. The work by Yeh et al. [6], nevertheless, does not directly estimate moisture content distributions with the consideration of the spatial variability in the constitutive resistivity-moisture content relation.

In this paper, an integrative algorithm based on a stochastic information fusion concept [7] is developed to provide the best unbiased estimate of moisture content distributions in the vadose zone by fusing both hydrological and geophysical information. The hydrological information includes point measurements of the moisture content and prior information about moisture content distributions (i.e., mean, variance and correlation structure.) The geophysical information consists of point measurements of electric potentials, parameters of the resistivity-moisture content relation, and prior information about spatial variability of these parameters. Numerical experiments were used to demonstrate the robustness of the integrative inverse approach for delineating transient moisture content distributions during a non-uniform infiltration event in three-dimensional heterogeneous vadose zones.

METHODOLOGY

Governing Equation for the Electric Potential

In a geological formation, the electric current flow induced by an electrical resistivity survey in general can be described by:

$$\nabla \cdot (\sigma(x)\nabla\phi(x)) + I(x) = 0 \quad \text{(Eq. 1)}$$

where ϕ is electric potential [v], I represents the electric current source density per volume [A/m^3], and σ is the electrical conductivity [S/m]. Electrical conductivity, σ, is the reciprocal of the electrical resistivity, ρ [Ωm], which is assumed to be locally isotropic. The boundary conditions associated with Eq. 1 are:

$$\phi\big|_{\Gamma_1} = \phi^* \quad \text{(Eq. 2)}$$

and

$$\sigma(x)\nabla\phi \cdot \underline{n}\big|_{\Gamma_2} = i \quad \text{(Eq. 3)}$$

where ϕ^* is the electric potential specified at boundary Γ_1, i denotes the electrical current density per unit area [A/m^2], and n is the unit vector normal to the boundary Γ_2.

Constitutive Resistivity and Moisture Content Relation

In this study, a power law relationship was used to relate resistivity to moisture content (e.g. [6]):

$$\rho = \rho_0 \theta^{-m} \quad \text{(Eq. 4)}$$

where ρ is bulk electrical resistivity, ρ_0 is a fitting parameter that is related to the electrical resistivity of pore water, m is a dimensionless fitting parameter, and θ denotes volumetric moisture content. We assume that ρ_0 does not change during an infiltration event in a field. Using Eq. 4, the linear relation between log resistivity before and after an infiltration can be expressed as:

$$\Delta \ln \rho(x) = -m(x)\Delta \ln \theta(x) \quad \text{(Eq. 5)}$$

According to this equation, the change of log resistivity ($\Delta ln\ \rho$) is linearly proportional to the change in log moisture content ($\Delta\ ln\ \theta$). If m is spatially invariant, the pattern of $\Delta ln\ \rho$(x) directly corresponds to the pattern of $\Delta ln\ \theta$ (x) in the entire field. On the other hand, if m is spatially variable and independent of $\Delta ln\ \theta$(x), the pattern of change seen in $ln\ \rho$ (x) does not directly correspond to the pattern of $\Delta ln\ \theta$ (x).

Furthermore, Eq. 5 is derived with the assumption that during an infiltration event ρ_0 remains constant, which may not always be valid. The resistivity of a porous medium can be highly variable, depending on the degree of saturation and the type of ions present in the pore water [13]. The spatial variability of ρ_0 and m may directly correspond to the pore water chemistry. Since silica, which comprises most mineral grains (except metallic ores and clays), is an insulator, the observed electrical conduction in porous media is mainly through interstitial pore water. When clay minerals are present, a relatively large number of ions may flow into or out of solution, through ion exchange, thus significantly changing the electrical conductivity of the fluid. During an infiltration event, other chemical reactions or processes may occur due to differences in water chemistry in the infiltrated water, thus altering the composition of ions present in pores and changing the nature of the pore electrolytes. This adds another level of spatial variability to the resistivity distribution.

Baker [9] measured electrical resistivity as a function of moisture content for core samples collected from a bore hole at the Sandia-Tech Vadose Zone (STVZ) infiltration field site in Socorro, New Mexico. A total of 25 samples were collected from eight 5-foot long continuous cores. The electrical resistivity values of the samples at several moisture contents were determined using an impedance analyzer. Eq. 4 was subsequently fitted to the measured resistivity and moisture data to determine the values for ρ_0 and m. Based on an analysis of the data set, Yeh et al. [6] reported that both $ln\ \rho_0$ and $ln\ m$ were approximately normally distributed. The geometric mean of ρ_0 is 7.036 Ωm and the variance, standard deviation, and the coefficient of variation for $ln\ \rho_0$ were 0.633, 0.796, and 40.8%, respectively. For m, the geometric mean was 1.336 (dimensionless), while variance, standard deviation, and the coefficient of variation for $ln\ m$ were 0.034, 0.185, and 63.7%, respectively. In addition, they found that both parameters are not entirely disordered in space but correlated over short distances. For $ln\ \rho_0$, an exponential variogram model was used to describe its spatial variability with sill, range, and nugget values of 0.8, 3.5 m, and 0.08, respectively. Similarly, an exponential variogram model was used for $ln\ m$. The sill, range, and nugget values for $ln\ m$ were 0.043, 3.5 m, and 0.01, respectively. No significant correlation between $ln\ \rho_0$ and $ln\ m$ was reported.

The observed spatial variability of $ln\ \rho_0$ and $ln\ m$ implies that equivalent changes in moisture content at different locations in the medium may lead to different changes in the measured electrical resistivity. As a result, the pattern of change in resistivity, detected by ERT surveys in a field, may not necessarily reflect the true pattern of change in the moisture content. To overcome this difficulty in interpreting ERT field surveys, we propose an integrative inverse algorithm that is based on the concept of stochastic information fusion developed by Yeh and ®im| nek [7].

Inverse (or Estimation) Algorithm

Since the parameters, ρ_0, θ, and m, vary spatially, and their specification at every point in space is practically impossible, they will be treated as random fields (e.g., [14, 15]), which are characterized by their statistical moments (i.e., means, variances, and correlation scales.) Note the fields can be either stationary or nonstationary stochastic processes. Accordingly, ρ and the electric potential ϕ are also treated as stochastic processes. In the following analysis, it is

assumed that $ln\ (\rho_0) = F + f$, $ln\ (\theta) = A + a$, $ln\ (m) = N + n$ and $\phi = H + h$, where F, A, N, and H are the mean values, and f, a, n, and h are the purtubations. The primary goal of the inverse (or estimation) algorithm is to estimate θ and ρ at any point in the three-dimensional geologic medium, although it can be used to estimate other parameters (i.e. ρ_0, m, and ϕ) as well. The estimation algorithm integrates point parameter measurements at several locations (including ρ_0, θ, and m,) and ERT measurements that consist of ϕ and the transmitted current density, I. Prior information about the means and covariances of ρ_0, θ, and m is also included; this information could be estimated from core samples, geological well logs, or outcrops.

Using first-order analysis, a state variable, such as ϕ, can be expanded in a Taylor series about the mean value of parameter. Neglecting the second and higher order terms of the Taylor series leads to a linear relation between the state variable and the parameters, χ_i:

$$\phi = \langle \phi \rangle + \sum_i \chi_i \left. \frac{\partial \phi}{\partial \chi_i} \right|_{\langle X_i \rangle \langle \phi \rangle} \qquad \text{(Eq. 6)}$$

For ERT surveys, $\chi_i = X_i - \langle X_i \rangle$ represents the zero mean perturbation of a natural log transformed parameter, such as $f = ln\ (\rho_0) - F$, $a = ln\ \theta - A$, and $n = ln\ m - N$; the zero mean perturbation of the state variable (i.e. electric potential) is $h = \phi - \langle \phi \rangle = \phi - H$; $\partial \phi / \partial \chi_i$ represent the sensitivity derivatives of electric potential with respect to the parameters, and are computed using an adjoint state method. Details of the derivation of these sensitivities can be found in Sun and Yeh [16], Li and Yeh [17] and Hughson and Yeh [18]. The sensitivity of the electric potential at location i to a perturbation in a parameter at location k can be generally expressed as:

$$\frac{\partial \phi_i}{\partial \chi_k} = \int_{\Omega_k} \frac{\partial \sigma}{\partial \chi} \nabla \langle \phi \rangle \cdot \nabla \Phi d\Omega \qquad \text{(Eq. 7)}$$

Specifically, the sensitivities for the parameters in this study are:

$$\frac{\partial \phi_i}{\partial f_k} = \int_{\Omega_k} \sigma \nabla \langle \phi \rangle \cdot \nabla \Phi d\Omega \qquad \text{(Eq. 8)}$$

$$\frac{\partial \phi_i}{\partial a_k} = \int_{\Omega_k} -m\sigma \nabla \langle \phi \rangle \cdot \nabla \Phi d\Omega \qquad \text{(Eq. 9)}$$

$$\frac{\partial \phi_i}{\partial n_k} = \int_{\Omega_k} -m \ln(\theta) \sigma \nabla \langle \phi \rangle \cdot \nabla \Phi d\Omega \qquad \text{(Eq. 10)}$$

where Ω_k is the domain of the element containing node k if a finite element approach is used and Φ represents the adjoint state variable, which can be solved for using the adjoint state equation:

$$\nabla \cdot (\sigma(x)\nabla\Phi) = \delta(x - x_k) \quad \text{(Eq. 11)}$$

where δ is the Dirac delta function, and x_k is the measurement location of the electric potential. Notice that the mean electric potential, $\langle\phi\rangle$, is needed to evaluate the sensitivities (see Eq. 8, 9, and 10.) The mean electric potential is derived by solving a mean equation that is of the same form as the Eq. 1 [6], with a mean electrical resistivity and moisture content relation that is the same as Eq. 4, but with the parameters set to their mean values.

Once the mean electric potential field is derived, the above sensitivity equations are used to calculate covariance of *h* and the cross-covariance between *h* and χ. Rewriting Eq. 6 in matrix form yields:

$$\{h\} = \sum_{\chi} J_{h\chi}\Big|_{H,\langle X\rangle} \{\chi\} \quad \text{(Eq. 12)}$$

where $\{\ \}$ indicates the vector of the descretized variable, $J_{h\chi}$ is a jacobian matrix representing the derivatives of the potential with respect to the parameters, i.e., $\partial\phi/\partial\chi_i$, which can be obtained using Eq. 8 through 10, and has dimensions of $n_h \times nelem$. The number of voltage measurement locations is given as n_h,and *nelem* is the total number of elements in the domain. Multiplying Eq. 12 by the transpose of $\{\chi\}$ (i.e. $\{f\}$, $\{a\}$, $\{n\}$) and $\{h\}$, and then taking the expectations on both sides, yields:

$$R_{h\chi} = J_{h\chi} R_{\chi\chi} \quad \text{(Eq. 13)}$$

$$R_{hh} = \sum_{\chi} J_{h\chi} R_{\chi\chi} J_{h\chi}^T$$

where superscript *T* denotes transpose; $R_{h\chi}$ represents the cross-covariance functions between *h* and *f*, *h* and *a*, or *h* and *n*, with dimensions of $n_h \times nelem$; $R_{\chi\chi}$ denotes the covariance functions of *f*, *a,* and *n* with dimensions of $nelem \times nelem$, and they are given a priori. A nugget can be added to the covariance to represent measurement errors, or variations within the sample scale if they are known. Because little information is available about the parameters, *f*, *a*, and *n* in the field, these parameters are assumed to be independent of each other in our study. Such an assumption merely represents the worst scenario in which knowledge of one variable does not provide any information about the others. R_{hh} in Eq. 13 represents the covariance function of *h*, which has dimensions of $n_h \times n_h$. Similarly, a nugget representing errors or variability due to scale disparity in potential measurements can be added to this covariance function.

Using these cross-covariance and covariance functions, a first-order estimate of the perturbations of the log transformed parameters is obtained by using the conditional expectation given observed primary information χ^* (i.e.ρ, ρ_0, and *m*) and secondary information h^* (θ and ϕ) collected during an ERT survey [19, 20]:

$$\hat{\chi} = \lambda_\chi{}^T \chi^* + \lambda_h{}^T h^* \quad \text{(Eq. 14)}$$

where $\hat{\chi}$ is a *nelem* long vector of the estimated purtabation of parameters, ρ_0 ,*m,* and θ; χ^* and h^* are perturbations of measured parameters and electrical potential, respectively; λ_χ and λ_h are weights (or cokriging weights in geostatistics) for the measurements, χ^* and h^* , respectively. They are evaluated as follows:

$$\begin{bmatrix} C_{\chi\chi} & C_{\chi h} \\ C_{h\chi} & C_{hh} \end{bmatrix} \begin{bmatrix} \lambda_\chi \\ \lambda_h \end{bmatrix} = \begin{bmatrix} C_{\chi\chi} \\ C_{h\chi} \end{bmatrix} \quad \text{(Eq. 15)}$$

where $C_{\chi\chi}$ represents the covariance of χ between measurement locations; C_{hh} represents the covariance of h between measurement locations; and $C_{h\chi}$ denotes cross-covariance between h and χ at measurement locations. The right-hand side of Eq. 15 consists of the covariance of χ between measurement locations and the estimate position, and the cross-covariance of h at measurement locations and χ at the estimate location. In other words, the weights used in the estimation are not only directly related to spatial correlation structures of parameters and state variables at measurement locations, but also the cross-correlations of the parameters and state variables, and correlation and cross-correlation between measurements and the location where the parameter is to be estimated. These matrices all are subsets of the covariance and cross covariance matrices in Eq. 13.

Equation 14 approximates the nonlinear relation between the parameter to be estimated and the measured electric potential by means of a linear first-order approximation. Thus, the equation cannot fully exploit electric potential measurements. To circumvent this problem, a successive linear estimator similar to that used by Yeh et al. [21], Zhang and Yeh [22], Hanna and Yeh [23], Vargas-Guzmán and Yeh [24], Hughson and Yeh [18], and Vargas-Guzmán and Yeh [25] is employed. That is:

$$\hat{\chi}^{(r+1)} = \hat{\chi}^{(r)} + \lambda_h^{(r)T} \left(\phi^* - \phi^{(r)} \right) \quad \text{(Eq. 16)}$$

where $\hat{\chi}^{(r+1)}$ and $\hat{\chi}^{(r)}$ represent the parameter estimated at iteration *r+1* and *r*, $\phi^{(r)}$ is the electric potential at the the measurement locations calculated from the forward simulation using parameters estimated at iteration r, and $\lambda_h^{(r)}$ is the weight at iteration *r*, which is determined from the following:

$$\varepsilon_{hh}^r \lambda_h^r = \varepsilon_{\chi h}^{(r)T} \quad \text{(Eq. 17)}$$

The solution to Eq. 17 requires knowledge of $\varepsilon_{hh}^{(r)}$ and $\varepsilon_{h\chi}^{(r)}$; they are estimated using the following approximations at each iteration:

$$\varepsilon_{hh}^{(r)} = \sum_{\chi} J_{h\chi}^{(r)} \varepsilon_{\chi\chi}^{(r)} J_{h\chi}^{T^{(r)}}$$
$$\varepsilon_{h\chi}^{(r)} = J_{h\chi}^{(r)} \varepsilon_{\chi\chi}^{(r)} \qquad \text{(Eq. 18)}$$

where $J_{h\chi}$ is the sensitivity matrix of $n_h \times nelem$ at iteration r, and superscript T stands for the transpose. At iteration $r = 0$, $\varepsilon_{\chi\chi}$ is given by:

$$\varepsilon_{\chi\chi}^{1} = R_{\chi\chi} - \tilde{R}_{\chi\chi}\lambda_{\chi} - \tilde{R}_{\chi h}\lambda_{h} \qquad \text{(Eq. 19)}$$

where $\tilde{R}_{\chi\chi}$ is a subset of $R_{\chi\chi}$. For $r \geq 1$, the residual covariances are evaluated according to

$$\varepsilon_{\chi\chi}^{(r+1)} = \varepsilon_{\chi\chi}^{(r)} - \varepsilon_{\chi h}^{(r)} \lambda_{h}^{(r)} \qquad \text{(Eq. 20)}$$

Notice that these residual covariances represent first-order approximates of the conditional covariances.

Once all three parameters, *f, a,* and *n*, are estimated by fully utilizing the potential data and direct measurement of the parameters (if any,) the electrical conductivity is then estimated using Eq. 4. Afterwards, the mean electric potential equation is solved again with the newly estimated electrical conductivity for a new electric potential field. Then, the maximum change of σ_{χ}^2 (the variance of the estimated parameters of *f*, *a*, and *n*) and the change in the largest potential misfit among all measurement locations between two successive iterations are evaluated. If both changes are smaller than prescribed tolerances, the iteration stops. If not, new values for $\varepsilon_{h\chi}$ and ε_{hh} are evaluated using Eq. 18. Eq. 17 is then solved to obtain a new set of weights that are used in Eq. 16 with $(\phi_j^* - \phi_j^{(r)})$ to obtain a new estimate of the parameters. A theoretical proof the convergence of the successive linear estimator is given in Vargas-Guzmán and Yeh [25].

The previous section describes the ERT inversion algorithm for only one set of primary and secondary information obtained in one DC transmission. This algorithm can simultaneously include all potential measurements collected during all DC transmissions in an ERT survey. However, the system of equations (Eq. 15 and 17) can become extremely large and ill conditioned, in which case stable solutions to the equations are difficult to obtain [18]. To avoid numerical difficulties in solving the large system of equations, the voltage data sets are included sequentially. The sequential algorithm used is similar to the one developed for use in hydraulic tomography inversion [10]. In essence, the proposed sequential approach uses the estimated electrical conductivity field, the ρ_o, m, and θ fields, and their covariances and cross-covariances, as prior information for the next estimation using new sets of current/voltage data from DC transmissions at different locations. Vargas-Guzmán and Yeh [24] and Yeh and ®im| nek [7] gave an illustrative example of the sequential approach and explained the necessity for updating the covariances and cross-covariances. The sequential inclusion of data sets from different DC transmissions continues until all data sets have been utilized. All data sets are fully processed by propagating the conditional first and second moments from one data set to another. Such a sequential approach allows accumulation of high-density secondary information obtained from

an ERT survey, while maintaining the covariance matrix at a manageable size that can be solved with minimal numerical difficulties.

Inversions of ERT surveys for environmental applications are generally ill posed since the number of parameters to be estimated is often much greater than the number of measurements of the state variable (see [7] for a discussion about necessary and sufficient conditions for a well-posed inverse problem). An ill-posed problem typically has an infinite number of global minima and solutions. Classical inverse algorithms (e.g., regularized least-squares approach, [8]) can only derive an estimated parameter field that produces an electric potential field honoring measurements at sampling locations and a smooth estimate at other locations. This smooth field, however, does not necessarily honor the characteristics of the spatial variability of the true parameters (e.g. mean, variance, and correlation structure.) On the other hand, our sequential/successive linear estimator is a conditional effective parameter approach [21, 23, 15, 7]. It aims to yield a parameter field that produces not only parameter values and state variables observed at measurement locations, but also conditional effective parameter values at locations where no measurements are available. The effective parameters are our estimates based on the spatial statistics of the parameter field and its cross-correlations with state variables using the governing equation for the electric potential but also for the fluid flow process. Discussions of advantages of the approach can be found in Yeh and ®im| nek [7].

NUMERICAL EXPERIMENTS

In the following numerical examples, we tested our inverse algorithm for transient infiltration into a three-dimensional, hypothetical vadose zone. Water movement was simulated at 1,000 and 50,000 minutes from the commencement of an infiltration event. The simulated moisture content distributions at these two times, $\theta_{1,000}$ and $\theta_{50,000}$, were used as the true moisture content fields; and their difference was denoted as the true moisture content change in the following analysis. Following generation of random fields of ρ_o and m, the true resistivity fields at 1,000 and 50,000 minutes were calculated using Eq. 4 with the generated ρ_o, m, $\theta_{1,000}$ and $\theta_{50,000}$ fields.

Next, ERT surveys were simulated using these two resistivity fields. After collecting voltage/current data sets, two different inverse approaches were used to interpret water flow due to the infiltration event. The first approach used the inverse model developed by Yeh et al. [6] based on electric potential measurements only, to derive resistivity fields at times of 1,000 and 50,000 minutes. Next, the change in resistivity from 1,000 to 50,000 minutes is computed. Finally, the estimated change in resistivity is used to interpret the change in moisture content. The second approach estimated moisture distribution at 50,000 minutes directly using our new integrative method.

The hypothetical site was assumed to be a cube, 200 cm on each side, consisting of 2,000 elements, 20 × 20 × 10cm in size. The unsaturated hydraulic properties of each element were assumed to be described by the Mualem-van Genuchten model [26]:

$$K(\psi) = K_s \left(1 - (|\alpha\psi|)^{(\beta-1)} \left[1 + (|\alpha\psi|)^{\beta}\right]^{-\gamma}\right)^2 / \left[1 + (|\alpha\psi|)^{\beta}\right]^{\gamma/2}$$
$$\theta(\psi) = (\theta_s - \theta_r)\left[1 + (|\alpha\psi|)^{\beta}\right]^{(-\gamma)} + \theta_r \quad \text{(Eq. 21)}$$

where $K(\psi)$ is the unsaturated hydraulic conductivity as a function of the pressure head, ψ; K_s is the saturated hydraulic conductivity; α and β are shape factors; $\gamma=(1-1/\beta)$; θ_s is the saturated moisture content, and θ_r is the residual moisture content. To represent heterogeneity, the parameters of Eq. 21 were assumed to be stochastic processes. Since spatial variations in θ_s and θ_r are generally negligible, both were treated as deterministic constants with values of 0.366 and 0.029, respectively. The parameters, *Ks,* α, and β for each element in the simulation domain were generated using a method by Gutjahr [27] with specified means, variances, and correlation structures as listed in Table I. These generated random fields are then denoted as the true distributions of the hydraulic parameters for the hypothetical site. Figures 1a, b and c show the generated *ln Ks*, *ln* α, and *ln* β fields, respectively.

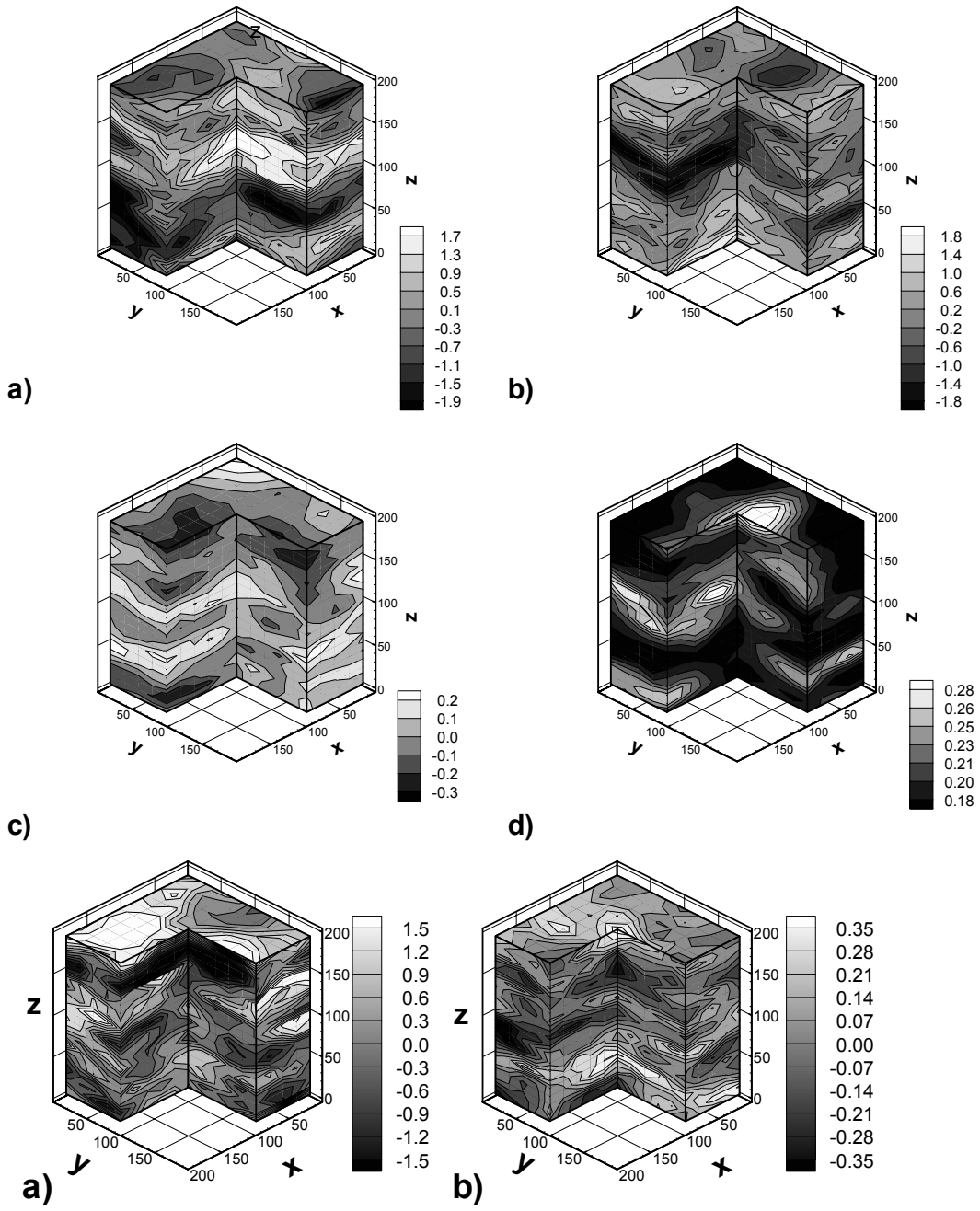

Fig. 1 a) Generated *ln Ks* field; b) Generated *ln* α field; c) Generated *ln* β field; d) True moisture content field at t =1,000 minutes, e) generated true *ln* ρ_o field; f) generated true *ln m* field.

Table I Hydrological and statistical parameters used in 3-D analysis

parameter	mean	variance	λx [cm]	λy [cm]	λz [cm]	Covariance model
Ks [cm/min]	0.043	0.893	80	80	20	Exponential
α [1/cm]	0.067	0.631	80	80	20	Exponential
β	1.811	0.015	80	80	20	Exponential

The initial pressure head condition was assumed to be hydrostatic. Specifically, the bottom was set at a prescribed pressure head of -50 cm, and the top was fixed at a pressure head of -250 cm. Infiltration occurred over an area of 1,600 cm^2 on the top center of the cube at a pressure head of -50 cm, while no-flux boundary conditions were assigned to the remainder of the top and the four sides. This created non-uniform vertical infiltration fields from a constant source on the top center of the flow domain. The infiltration process was simulated using a finite element model [28] to obtain moisture distributions. Figure 1d shows the moisture content distribution 1,000 minutes after infiltration began. Mean moisture content distributions at 1,000 and 50,000 minutes were similarly obtained with effective mean values of the hydraulic parameters. True changes in *ln θ* were computed as the differences between the true *ln θ* distributions at 1,000 and 50,000 minutes (Fig. 3a).

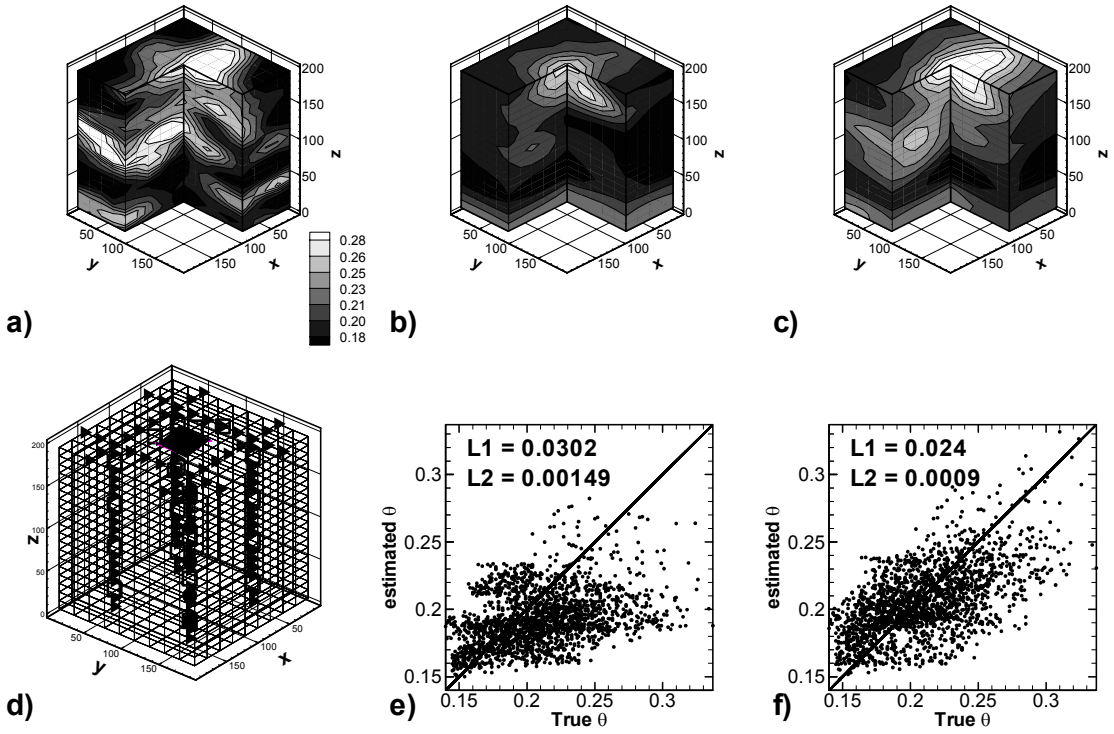

Fig. 3 a) True moisture content *θ* at t = 50,000 minutes; b) Estimated *θ* at t= 50,000 minutes without *θ* measurements; c) Estimated *θ* at t= 50,000 minutes with 20 *θ* measurements; d) Schematic diagram for 3-D ERT experiments, top center square indicates the infiltration area, right triangles indicate voltage measurement locations, circles show current source locations, and squares show the locations of 20 *θ* measurements; e) The scatter plot corresponding to b); f) The scatter plot corresponding to c).

To represent spatial variability in the parameters of the resistivity and moisture content relation in the field, the two parameters, ρ_o and m were considered as random fields with geometric means of 7.036 Ωm and 1.336, respectively. Variances of $ln\ \rho_o$ and $ln\ m$ were assumed to be 0.633 and 0.034, respectively. We again assumed that both parameters possessed the same exponential correlation structure with a horizontal correlation scale of 80 cm and a vertical correlation scale of 20 cm. Figures 1e and f show the generated true fields for these two parameters.

Based on these synthetic ρ_o, m, $\theta_{1,000}$ and $\theta_{50,000}$ fields, true synthetic resistivity fields at times of 1,000 and 50,000 minutes ($\rho_{1,000}$ and $\rho_{50,000}$, respectively) were calculated using Eq. 4. ERT surveys were then simulated using these two resistivity fields. Figure 3d displays the three-dimensional layout of the ERT survey. The design of the ERT survey included four bore holes penetrating the entire depth of the site domain. The x and y coordinates pairs, in centimeters, of the four bore holes were (50, 50), (150, 50), (50, 150), and (150, 150). Twenty electrodes were installed along each bore hole. Electrodes were also deployed along the surface in four lines with endpoints at the above x-y coordinates. Current sources were installed along the upper right bore hole (150, 150) at the five depths of 25, 55, 95, 135, and 175 cm. Using the same collection precedure for the voltage data as used for the 2-D numerical examples, five ERT voltage data sets of 111 voltage measurements each were obtained. In addition, 20 ρ_o and m values along each of the four bore holes (a toal of 80 measurements) were assumed to be available for our analysis, while θ was sampled at 20 locations indicated by squares in Fig. 3d. To investigate the effect of direct θ measurements on the inverted estimate of the moisture content at the site, the moisture content distribution at 50,000 minutes was estimated without any θ measurement and compared to the estimate with 20 θ measurements.

Using Resistivity Change to Interpret Water Flow.

For the purpose of comparison, resistivity changes were computed to reflect water movement in vadose zone. Forward simulations of ERT surveys based on the previously discussed network layout were conducted using the simulated moisture distributions at 1,000 and 50,000 minutes. Five voltage data sets were collected and then used in the inverse approach of Yeh et al. [6] to estimate the resistivity fields at these two specified times. The change in resistivity between 1,000 and 50,000 minutes was then computed. Figure 2a displays the pattern of the true moisture content change, and Fig. 2b the estimated pattern of resistivity change. A comparison of these two figures indicates that interpretation of water movement based on the pattern of the estimated resistivity change alone led to incorrect estimates of water flow. Between 1,000 and 50,000 minutes, the true water front moved in a south-west direction, while the estimated pattern of resistivity change suggests flow in a south-eastern direction. Two factors contribute to this discrepency: uncertainty in the estimated resistivity fields, caused by a limited number of voltage measurements and spatial variability in the parameters of the resistivity-moisture content relationship (especially in parameter m). According to Eq. 5, the pattern of the change in resistivity in the domain is proportional to that of changes in the moisture content by a constant m. If m is not spatial invariant, the pattern of changes in the resistivity will not resemble those in the moisture content. Thus, a detailed spatial distribution of the parameter must be known to correctly relate changes in the resistivity to those in the moisture content. The more variability m is, the greater the difference between the pattern of moisture change and that of the resistivity

change will be. Relying only on changes in resistivity and neglecting spatial variability in the parameters of the resistivity-moisture content relationship can undoubtedly lead to erroneous flow directions and patterns.

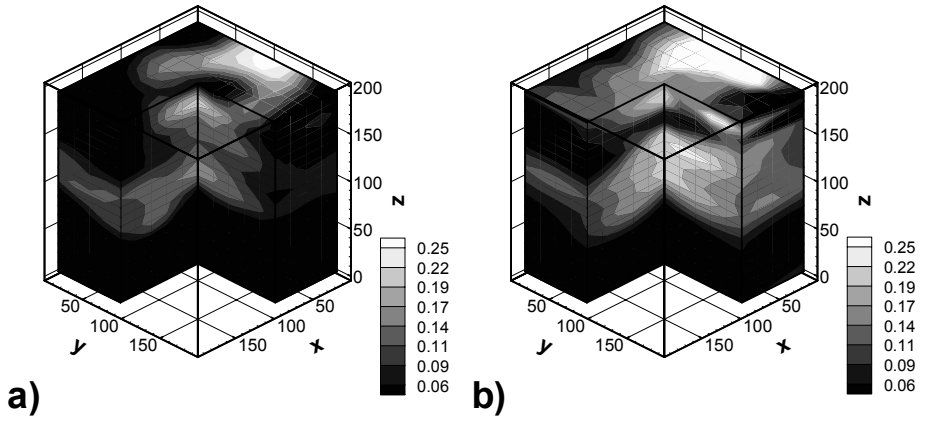

Fig. 2. a) True $\Delta ln\ \theta$ from 1,000 to 5,000 minutes; b) Estimated $\Delta ln\ \rho$ from 1,000 to 50,000 minutes.

Directly Estimation of Moisture content Distribution.

Figures 3a and b show the true moisture content distribution at 50,000 minutes and the corresponding estimated moisture content distribution using 111 × 5 voltage measurements, and 80 ρ_o and m measurements. The estimated field using the same number of voltage, ρ_o and m measurements, but also including 20 direct θ measurements, is illustrated in Fig. 3c. Comparisons of the three figures show that the proposed inverse algorithm reproduces the general pattern of the simulated true moisture content distribution, even though the constitutive relation between resistivity and moisture varies spatially. The inclusion of the 20 θ measurements, in particular, greatly improves the estimates of the θ distribution. Figures 3e and f are scatter plots corresponding to Fig.s 3b and c, respectively; a 45^o line indicates perfect estimation. The goodness of fit was also evaluated using L1 and L2 norms. The reduction in the L1 and L2 norms from Figs. 3e to f suggests that the addition of moisture content measurements dramatically improve the estimate. The conditional variance of the estimate from our stochastic fusion approach can be used to assess the uncertainty associated with the estimate: a smaller conditional variance indicates less uncertainty in the estimate. The conditional variances corresponding to the estimates by using zero and 20 θ measurements are shown on Figs. 4a and b, respectively. Small conditional variances are located closely to the four bore holes where secondary information is measured. At locations where moisture content measurements were collected, the conditional variance is zero, indicating that these observations are honored in the inverse model and that no uncertainty exists.

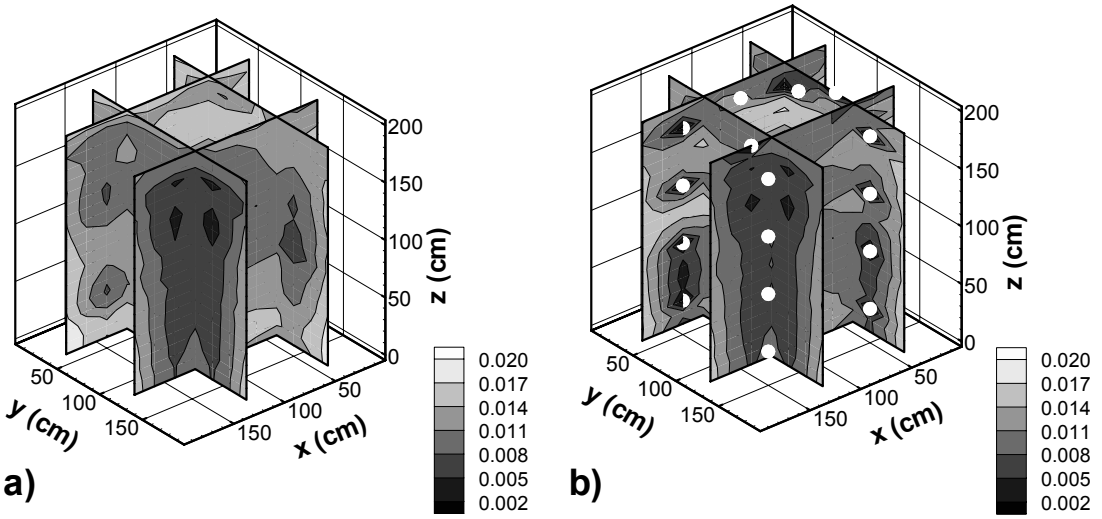

Fig. 4. a) Conditional variance when no θ measurements are used at t= 50,000 minutes; b) Conditional variance when 20 θ measurements are used at t= 50,000 minutes. Circles indicate θ measurement locations

CONCLUSION

Knowledge of detailed moisture content distributions is important to our unstanding of vadose zone processes and water resouces management. An ERT inversion based on the concept of stochastic information fusion is developed to directly estimate moisture content distributions in a three-dimensional vadose zone. The approach integrates point measurements of electric potential, parameters of the constitutive relation between moisture and resistivity, and moisture content. In addition, the approach includes prior information about the spatial statistics of the moisture content distribution and the paramters of the constitutive relation.

Numerical examples illustrate that interpretations of water movement in the subsurface, based on only the estimated resistivity changes, can be misleading, due to spatial variability in the resistivity-moisture content relation parameters. Numerical examples also demonstrate the ability of the integrative ERT survey inverse model for estimating moisture contents directly. The model yields good estimates at the locations where primary and secondary information is measured. Primary information (i.e., the moisture measurements) contributes significantly to the accuracy of the estimated moisture content distribution. A large number of potential measurements are useful but they did not dramatically improve the estimate. This further supports the finding by Yeh et al. [6] that potential measurements alone are inadequate to characterize water flow in vadose zone. Finally, we conclude that fusing geophysical measurements with hydrological information using a stochastic approach is necessary to yield hydrologically realistic results under field conditions and to quantify uncertainty associated with the results.

ACKNOWLEDGEMENTS

This research was funded in part by a DOE EMSP96 grant through Sandia National Laboratories (Contract AV- 0655#1), a DOE EMSP99 grant through University of Wisconsin, A019493, and NSF and SERDP grant EAR-0229717. We also thank Kris Kuhlman for his technical editing.

REFERENCES

1 Daily, W, A. Ramirez, D. LaBrecque and J. Nitao, 1992, Electrical Resistivity Tomography of Vadose Water Movement, Water Resour. Res., 28(5), 1429-1442.

2 Ellis, R.G., and S.W. Oldenburg, 1994, The Pole-Pole 3D DC Resistivity Inverse Problem: A Conjugate Gradient Approach, Geophysical journal international 119,187-194.

3 Li, Y., and D.W. Oldenburg, 1994, Inversion of 3D dc-resistivity data using an approximate inverse mapping, Geophysical journal international 116, 527-537.

4 Zhang, J., R.l. Mackie, and T. Madden, 1995, 3-D resistivity forward modeling and inversion using conjugate gradients. Geophysics 60, 1313-1325.

5 Zhou, Q. Y., J. Shimada, and A. Sato, 2001, Three-dimensional spatial and temporal monitoring of soil water content using electrical resistivity tomography, Water Resour. Res., 37(2), 273-285.

6 Yeh, T. -C. J., and S. Liu, R. J. Glass, K. Baker, J. R. Brainard, D. Alumbaugh, D. LaBrecque, 2002, A geostatistically based inverse model for electrical resistivity surveys and its applications to vadose zone hydrology, Water Resour. Res., Vol. 38, No. 12, 1278, doi: 10.1029/2001WR001024.

7 Yeh, T.-C. J. and J. ®im| nek, 2002, Stochastic fusion of information for characterizing and monitoring the vadose zone, Vadose Zone Journal, 1:207-221.

8 Tikhonov, A. N., 1963, Resolution of ill-posed problems and the regularization method (in Russian), Dokl. Akad. Nauk SSSR, 151, 501-504.

9 Baker, K., 2001, Analysis of hydrological and electrical properties at the Sandia-Tech Vadose Zone Facility, Master Thesis, New Mexico Tech., Socorro, NM.

10 Yeh, T.-C. J., Liu, S.Y., 2000, Hydraulic tomography: Development of a new aquifer test method, Water Resour. Res., 36(8), 2095-2105.

11 Bohling, G. C. X. Zhan, J. Butler Jr., and L. Zheng, 2002, Steady shape analysis of tomographic pumping tests for characterization of aquifer heterogeneities, Water Resour. Res.38(12), 60-1 to 60-15.

12 Liu, S., T. -C. J. Yeh and R. Gardiner, 2002, Effectiveness of Hydraulic Tomography: Numerical and Sandbox Experiments, Water Resour. Res.,38(4), 10.1029/2001WR000338.

13 Sharma, Perm V., 1997, Environmental and engineering geophysics, Cambridge University Press.

14 Yeh, T.-C. J., 1992, Stochastic modeling of groundwater flow and solute transport in aquifers, J. of Hydrologic Processes, Vol. 6, 369-395.

15 Yeh, T.-C. J., 1998, Scale issues of heterogeneity in vadose-zone hydrology, in Scale Dependence and Scale Invariance in Hydrology, edited by G. Sposito, Cambridge Press.

16 Sun, N-Z., and W. W.-G. Yeh, 1992, A stochastic inverse solution for transient groundwater flow: parameter identification and reliability analysis, Water Resour. Res., 28(12), 3269-3280.

17 Li, B., and T.-C. J. Yeh, 1998, Sensitivity and moment analysis of head in variably saturated regimes, Adv. Water Resour., 21, 477-485.

18 Hughson, D. L., and T.-C. J. Yeh, 2000, An inverse model for three-dimensional flow in variably saturated porous media, Water Resour. Res., 36(4), 829-839.

19 Priestley, M. B., 1989, Spectral Analysis and Time Series, Academic Press, pp 890.

20 Yeh, T.-C. J., and J. Zhang, 1996, A geostatistical inverse method for variably saturated flow in the vadose zone, Water Resour. Res., 32(9), 2757-2766.

21 Yeh, T.-C. J., M. Jin, and S. Hanna, 1996, An iterative stochastic inverse method: conditional effective transmissivity and hydraulic head fields, Water Resour. Res., 32(1), 85-92.

22 Zhang, J., and T.-C. J. Yeh, 1997, An iterative geostatistical inverse method for steady flow in the vadose zone, Water Resour. Res., 33(1), 63-71.

23 Hanna, S. and T.-C. J. Yeh, 1998, Estimation of co-conditional moments of transmissivity, hydraulic head, and velocity fields, Advances in Water Resour. , 22(1), 87-93.

24 Vargas-Guzmán, J.A., and T.-C. J. Yeh, 1999, Sequential kriging and cokriging: two powerful geostatistical approaches, Stochastic Environmental Research and Risk Assessment, 13(6), 416-435.

25 Vargas-Guzmán, J.A., and T.-C. J. Yeh, 2002, The successive linear estimator: a revisit, Adv. Water Resour. 25: 773-781.

26 van Genuchten, M. T., 1980, A closed-form equation for predicting the hydraulic conductivity of unsaturated soils. Soil Sci. Soc. Am. J. 44, 892-898.

27 Gutjahr, A., 1989, Fast Fourier transforms for random field generation, N. M. Tech Project Report, 106 pp.

28 Srivastava, R., and T.-C. J. Yeh, 1992, A three-dimensional numerical model for water flow and transport of chemically reactive solute through porous media under variably saturated conditions. Adv. Water Resour., 15(5), 275-287.